Electronic Supplementary Material (ESI) for Journal of Materials Chemistry A.

Ultrahigh-performance tungsten-doped perovskites for the oxygen evolution reaction

Gao Chen, Zhiwei Hu, Yanping Zhu, Zhi-Gang Chen, Yijun Zhong, Hong-Ji Lin, Chien-Te Chen, Liu Hao Tjeng, Wei Zhou* and Zongping Shao*

Catalyst preparation. $SrCo_{0.8-x}Fe_{0.2}W_xO_{3-\delta}$ powders were prepared via a combined sol-gel route. Briefly, stoichiometric amounts of $Sr(NO_3)_2$, $Co(NO_3)_2 \cdot 6H_2O$, $Fe(NO_3)_3 \cdot 9H_2O$ and $(NH_4)_{10}W_{12}O_{41}$ (all of analytical grade, Sinopharm Chemical Reagent Co., Ltd.) were dissolved in deionized water, followed by the addition of a mixed solution of EDTA ($C_{10}H_{16}N_2O_8$, Sinopharm Chemical Reagent Co., Ltd.) and citric acid ($C_6H_8O_7$, Sinopharm Chemical Reagent Co., Ltd.) as complexing agents at a molar ratio of 1:1:2 for the total metal ions/EDTA/citric acid. To ensure complete complexation, an aqueous ammonium hydroxide solution ($NH_3 \bullet H_2O$, 28%, Sinopharm Chemical Reagent Co., Ltd.) was added to adjust the solution pH value to approximately 6. The solution was continuously stirred and evaporated at 90 ^oC to yield a clear transparent gel. The gel was then heated in a furnace at 250 ^oC for 5 h to form a solid precursor. Further calcination in air at 1000 ^oC for 10 h was conducted to obtain the perovskite powders.

Physicochemical characterization. The obtained samples were characterized by room temperature (RT) powder diffraction for phase identification and to assess phase purity. A diffractometer (Rigaku Smartlab, Cu Kα radiation, λ =1.5418 Å) with a Bragg-Brentano reflection geometry was used. The diffraction patterns were recorded by continuous scanning in the 2θ range of 10–90 ° at an interval of 0.02 °. Structural refinements of the XRD patterns were carried out using DIFFRAC plus Topas 4.2 software. During the refinements, general parameters such as the scale factor, background parameters, and the zero point of the counter were optimized. A Le Bail refinement was used initially to determine the space group and to approximate the lattice parameters of the SCFW catalysts. The Rietveld refinement was then performed to determine the general position of the atoms. The specific surface areas of the catalysts were obtained with a Brunauer-Emmet-Teller (BET) analysis system with a N_2 adsorptive medium. Transmission electron microscopy (TEM) was

conducted at 200 kV with a Philips Tecnai T30F field emission instrument equipped with a 2k-CCD camera. The X-ray absorption near-edge structure (XANES) spectra were measured at the BL17A beamline and the soft X-ray absorption spectroscopy (XAS) spectra were measured at the BL11A beamline of the National Synchrotron Radiation Research Center (NSRRC) in Taiwan. The Co−L and Fe-L XAS spectra were taken in the total electron yield mode. Clean sample surfaces were obtained by cutting pellets in situ just before collecting the data in an ultrahigh vacuum chamber with a pressure in the low 1×10^{-9} mbar range.

Electrode preparation and electrochemical characterization. Electrochemical measurements were performed at room temperature using a rotating disk working electrode made of glassy carbon (PINE, 5 mm diameter, 0.196 cm^2) connected to a CHI 760 E electrochemical station. The glassy carbon (GC) electrode was prepolished with 50 nm α-Al_2O_3 slurries on a polishing cloth and sonicated in ethanol for 5 min. The electrodes were finally rinsed with deionized water and dried before each test. A Pt foil and Ag/AgCl (3.5 M KCl) were used as the counter and reference electrodes, respectively. The potentials reported in our work are references to the reversible hydrogen electrode (RHE), 0.95 V. The calibration was performed in a high purity hydrogen saturated electrolyte with a platinum rotating disk electrode as the working electrode. CV was cycled at a scan rate of 1 mV s^{-1}, and the average of the two potentials at which the current crossed zero was taken to be the thermodynamic potential for the hydrogen electrode reaction. The preparation method of the working electrodes containing the investigated catalysts is stated as follows. To remove any electrode conductivity limitation present in the thin film electrodes, all the catalysts were mixed with as-received conductive carbon (Super P Li) at a mass ratio of 1:1. Briefly, the electrocatalyst suspensions were prepared by sonication of a mixture of oxide (10 mg), conductive carbon (10 mg), Nafion solution (5 wt%, 100 μL) and ethanol (1 mL) for at least 1 h to generate homogeneous ink. Next, a 5 μL aliquot of the as-prepared catalyst ink was dropped onto the surface of the RDE, yielding an approximate catalyst loading of 0.464 mg_{total} cm^{-2} (0.232 mg_{cat} cm^{-2}) and left to dry for the OER tests. The electrolyte was a 0.1 M KOH aqueous solution (99.99% metal purity),

which was saturated with O_2 for ~30 min prior to each test and maintained under an O_2 atmosphere throughout. Linear sweeping voltammograms (LSVs) were performed at the RDE at 1600 rpm in an O_2-saturated 0.1 M KOH solution at a scan rate of 5 mV s^{-1} from 0.2 to 1.0 V versus Ag|AgCl (3.5 M KCl). All potential values are iR-corrected to compensate for the effect of the solution resistance, which was calculated by the following equation: $E_{iR\text{-}corrected} = E - iR$, where i is the current and R is the uncompensated ohmic electrolyte resistance (~40 Ω) measured via the high-frequency ac impedance in O_2-saturated 0.1 M KOH.

Calculation of the metal-oxygen bond energy.

The individual <A-O> and <B-O> metal-oxygen bond energy within the perovskite lattice were calculated as follows:

$$<A-O> = \frac{1}{CN_A * m} * (\Delta^{H_{A_mO_n}} - m * \Delta^{H_A} - \frac{n}{2} * D_{O_2} \quad (1)$$

$$<B-O> = \frac{1}{CN_B * m} * (\Delta^{H_{B_mO_n}} - m * \Delta^{H_B} - \frac{n}{2} * D_{O_2} \quad (2)$$

where $\Delta^{H_{A(B)_mO_n}}$ and $\Delta^{H_{A(B)}}$ represent the enthalpy of formation of one mole of $A(B)_mO_n$ and the sublimation energy of A(B) metal obtained from the thermodynamic data at 25 °C, respectively. $CN_{A(B)}$ is the coordination number of cations at the A and B sites (CN_A=12, CN_B=6, respectively). D_{O2} is the dissociation energy of O_2 (e.g., 500.2 kJ mol^{-1}). ΔH_{SrO} = -591.5 kJ mol^{-1}, ΔH_{Sr} = 163.9 kJ mol^{-1}; ΔH_{Co2O3} = -653.1 kJ mol^{-1}, ΔH_{Co} = 428.0 kJ mol^{-1}; ΔH_{Fe2O3} = -820.5 kJ mol^{-1}, ΔH_{Fe} = 415.7 kJ mol^{-1}; ΔH_{WO3} = -842.9 kJ mol^{-1}, ΔH_W = 851.0 kJ mol^{-1}.

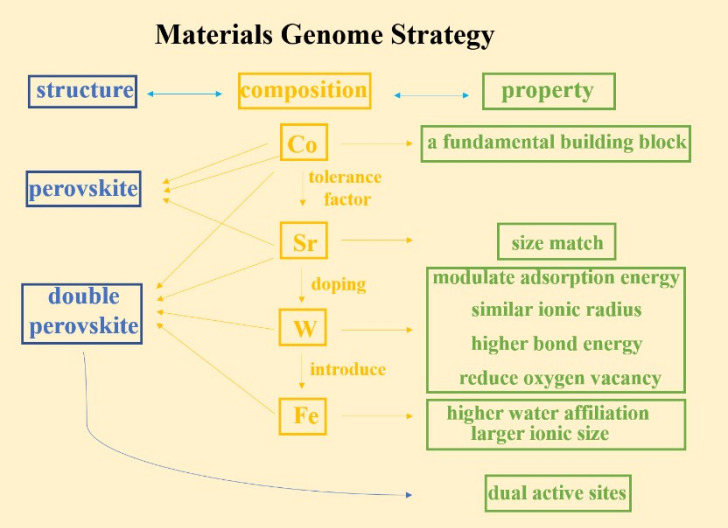

Figure S1. The visualized schematic diagram of the materials genome strategy.

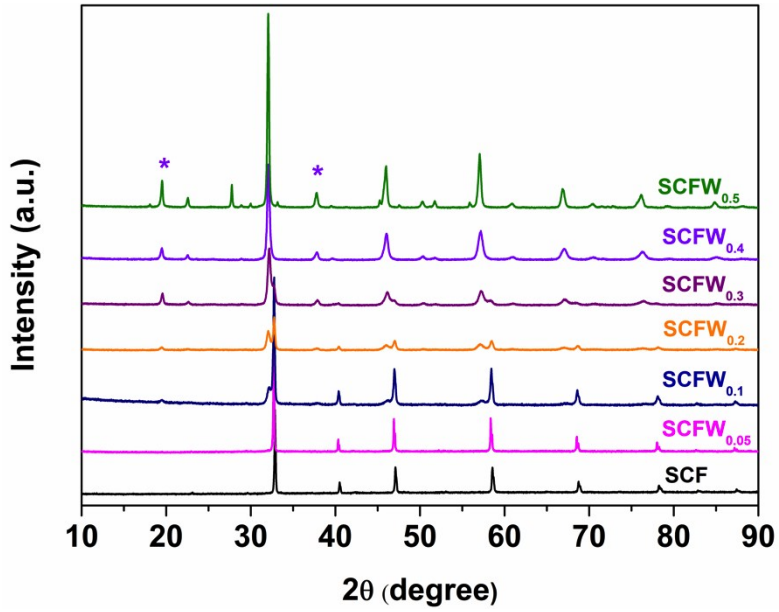

Figure S2. XRD patterns of the as-synthesized SCFW powders with various W content, in which the $SCFW_x$ (x=0.05, 0.1, 0.2, 0.3, 0.4 and 0.5) represents the materials with the nominal composition of $SrCo_{0.8-x}Fe_{0.2}W_xO_3$.

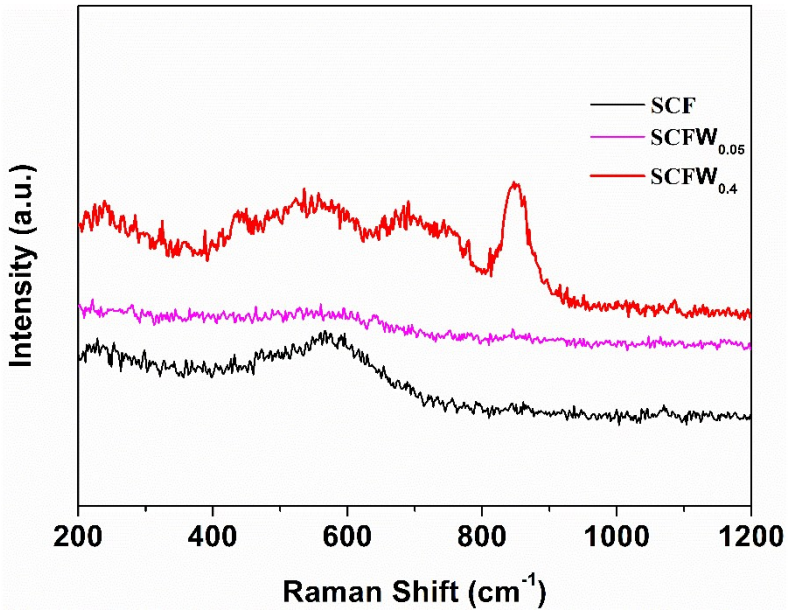

Figure S3. Raman spectra of the SCF, $SCFW_{0.05}$ and $SCFW_{0.4}$ samples.

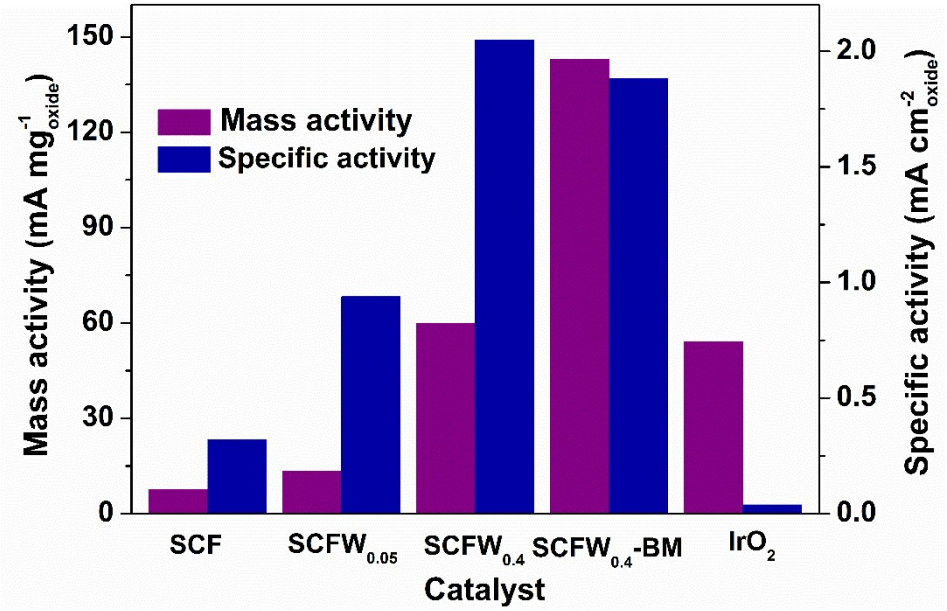

Figure S4. Mass activity and specific activity of the SCF, $SCFW_{0.05}$, $SCFW_{0.4}$, $SCFW_{0.4}$-BM and IrO_2 catalysts at an overpotential of η=0.41 V.

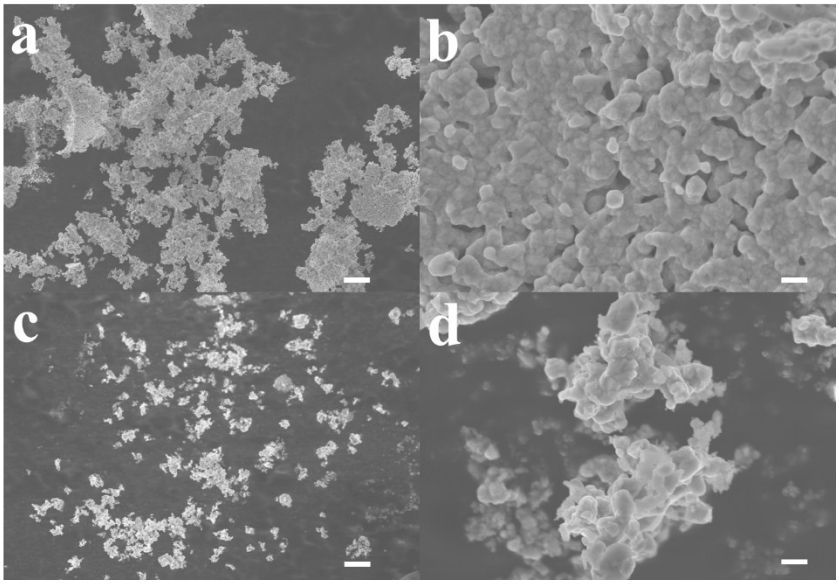

Figure S5. SEM images of $SCFW_{0.4}$ before (**a** and **b**) and after (**c** and **d**) ball-milling. The scale bars in **a** and **c** are 4 μm, in **b** and **d** are 0.4 μm.

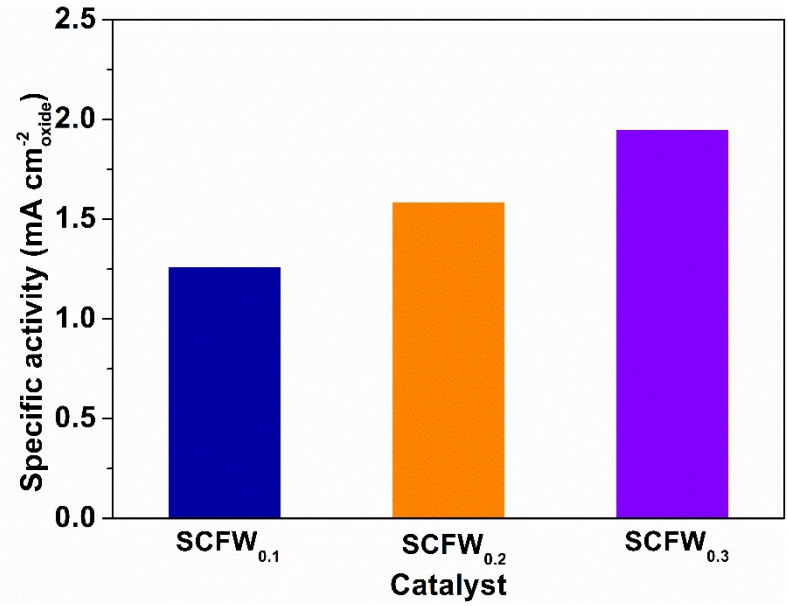

Figure S6. Specific activity of $SCFW_{0.1}$, $SCFW_{0.2}$ and $SCFW_{0.3}$ at an overpotential of η=0.41 V.

The calculation of the TOF (calibrated to the total amount of Co and Fe surface active sites)

Details concerning the calculation of the turnover frequency (TOF) per the surface Co and Fe atoms of the SCF, $SCFW_{0.05}$ and $SCFW_{0.4}$ samples are provided below.

First, the surface densities of the Co and Fe atoms (N_{ds}) in the studied catalysts were calculated through the unit-cell parameters. For SCF single perovskite with a cubic structure and unit-cell parameters of a=3.8456 Å with 1 B-site atom (Co+Fe) showing on a face, the density of the surface active sites (Co+Fe) was calculated to be 6.76×10^{14} atoms/cm^2. For $SCFW_{0.05}$ single perovskite with a cubic structure and unit-cell parameters of a=3.8682 Å with 1 B-site atom (Co+Fe+W) showing on a face, the density of the surface active sites (Co+Fe) was calculated to be 6.35×10^{14} atoms/cm^2. For $SCFW_{0.4}$ double perovskite with a tetragonal structure and unit-cell parameters of a = 5.5766 Å and c = 7.9346 Å with 2 B-site atoms (Co+Fe+W) showing on a face, the density of the surface active sites (Co+Fe) was calculated to be 2.71×10^{14} atoms per square centimetre.

Second, the surface area (*S*) of the samples was measured by nitrogen adsorption testing using the BET method (see **Table S1**).

Third, the mass loading (*m*) on glassy carbon (GC) is 0.045 mg_{cat} for all samples (see the **Electrode preparation and electrochemical characterization**).

Hence, the number of the surface Co and Fe atoms on the electrode is calculated by the equation: $Ns=N_{ds}\times S\times m$, where N_{ds} is the density of surface Co and Fe atoms in the studied catalysts, *S* is the surface area of the studied catalysts, and *m* is the mass loading.

Ns for SCF $=10\times6.76\times10^{14}\times2.3915\times0.045$

$=7.27\times10^{14}$ atoms

Ns for $SCFW_{0.05}$ $=10\times6.35\times10^{14}\times1.4259\times0.045$

$=4.08\times10^{14}$ atoms

Ns for $SCFW_{0.4}$ $=10\times2.71\times10^{14}\times2.9231\times0.045$

$=3.57\times10^{14}$ atoms

Finally, the turnover frequency (TOF) was calculated according to the relation:

TOF = J*A/(4*F*n)

where J is the current density at an overpotential of 0.41 V, A is the surface area of the electrode, F is Faraday's constant and n is the number of moles of surface cobalt and iron atoms ($n=N_s/N_A$, where N_A is Avogadro's constant).

TOF for SCF = $(1.4393\times10^{-3}\times0.196)/(4\times96485.3\times7.27\times10^{14}/(6.02\times10^{23}))$

$=0.75\ s^{-1}$

TOF for $SCFW_{0.05}$ = $(2.5082\times10^{-3}\times0.196)/(4\times96485.3\times4.08\times10^{14}/(6.02\times10^{23}))$

$=2.36\ s^{-1}$

TOF for $SCFW_{0.4}$ = $(10.3980\times10^{-3}\times0.196)/(4\times96485.3\times3.57\times10^{14}/(6.02\times10^{23}))$

$=11.90\ s^{-1}$

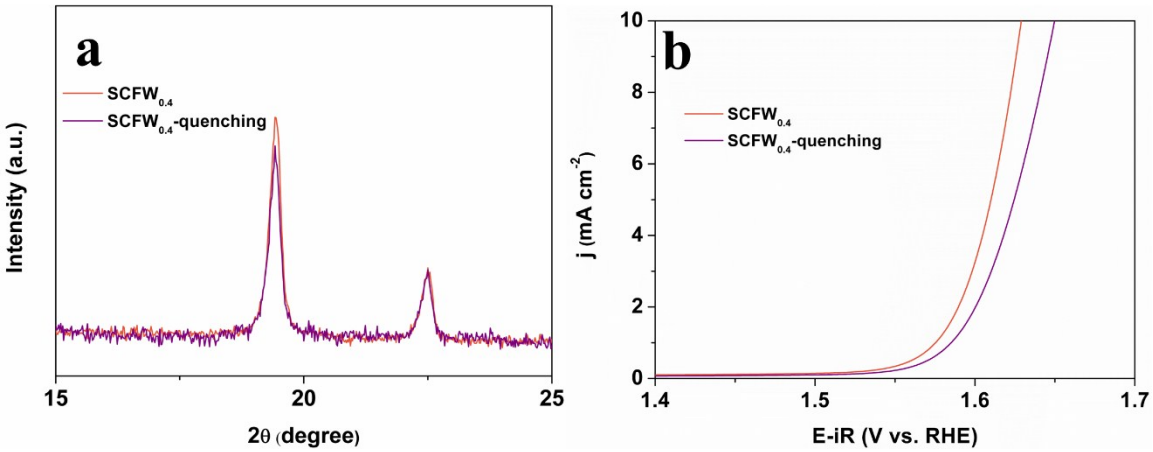

Figure S7. (**a**) The XRD patterns of $SCFW_{0.4}$ and $SCFW_{0.4}$-quenching and (**b**) the OER activity of $SCFW_{0.4}$ and $SCFW_{0.4}$-quenching.

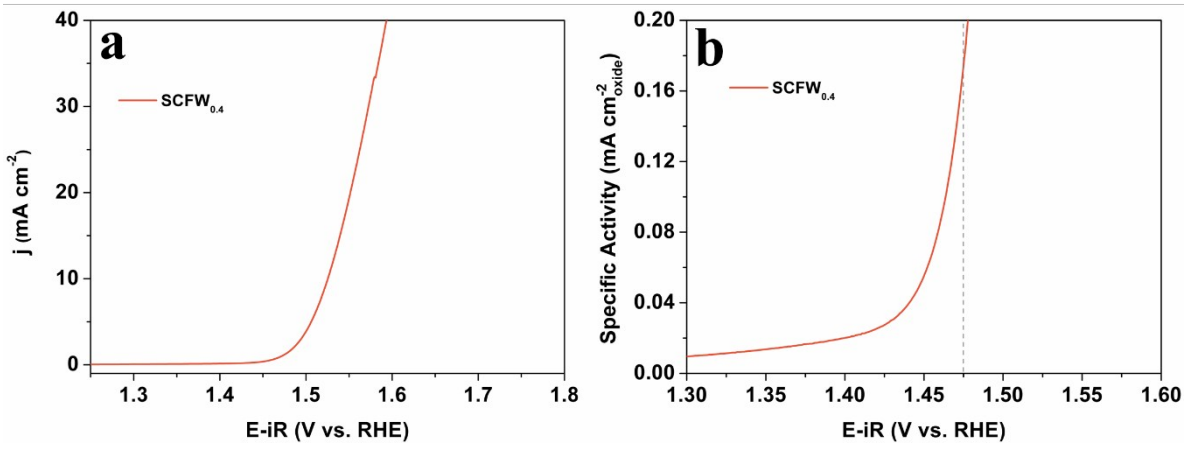

Figure S8. (**a**) LSV curve of the $SCFW_{0.4}$ catalysts in an O_2-saturated 1 M KOH solution at 1600 rpm and (**b**) the corresponding intrinsic activity.

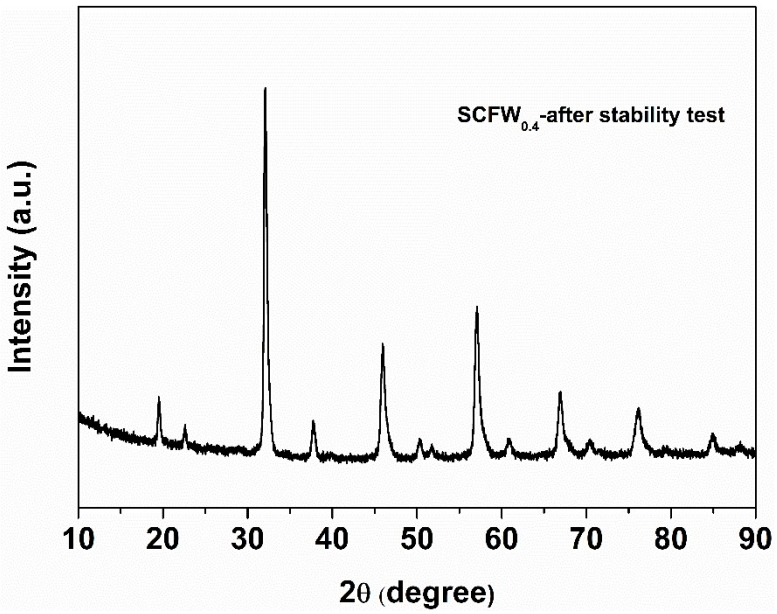

Figure S9. XRD pattern of the $SCFW_{0.4}$ sample after stability test.

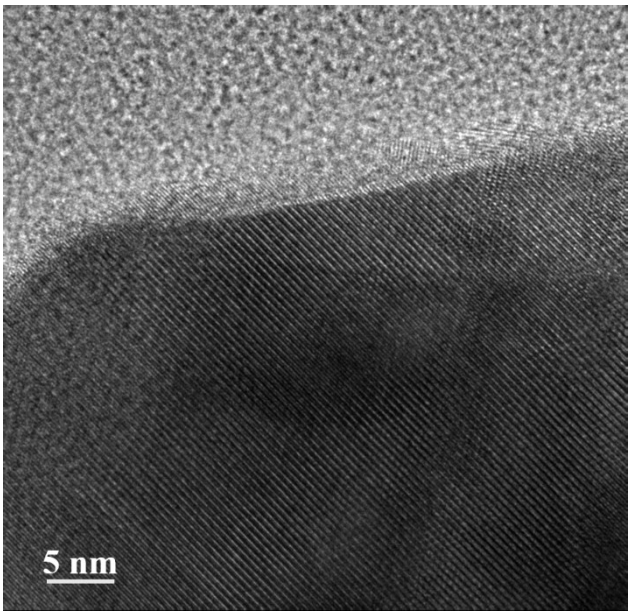

Figure S10. The HRTEM image of the $SCFW_{0.4}$ electrocatalyst after stability test.

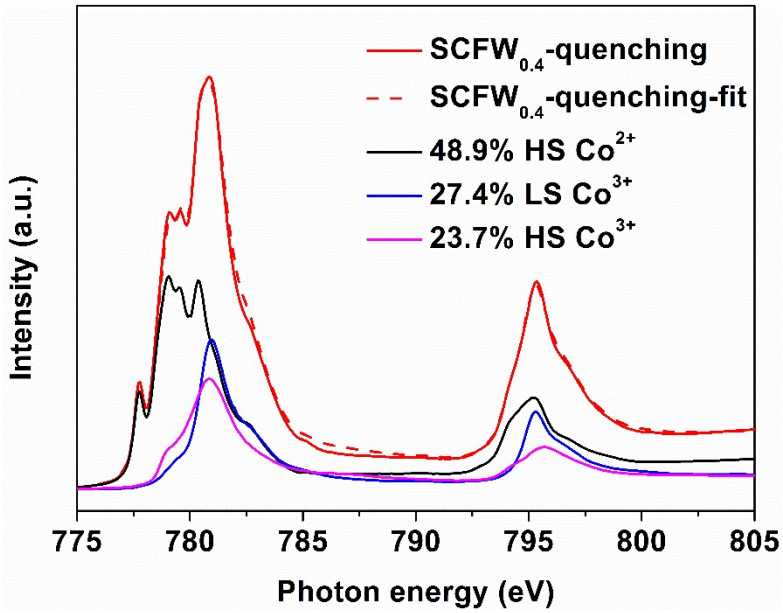

Figure S11. Simulations of the Co $L_{2,3}$ XAS spectra of $SCFW_{0.4}$-quenching together with references used.

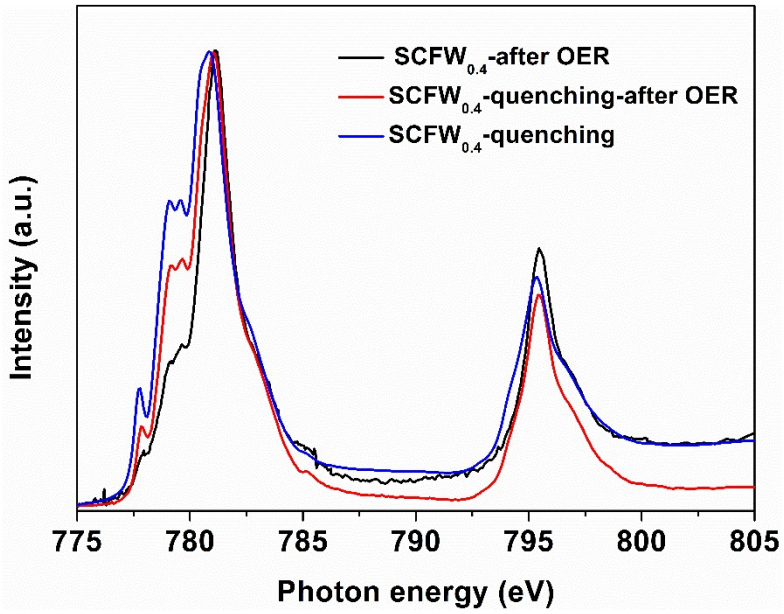

Figure S12. The Co $L_{2,3}$ XAS spectra of $SCFW_{0.4}$ after OER (black), quenched $SCFW_{0.4}$ after OER(red), SCW after OER (blue) and quenched $SCFW_{0.4}$ before the OER (green).

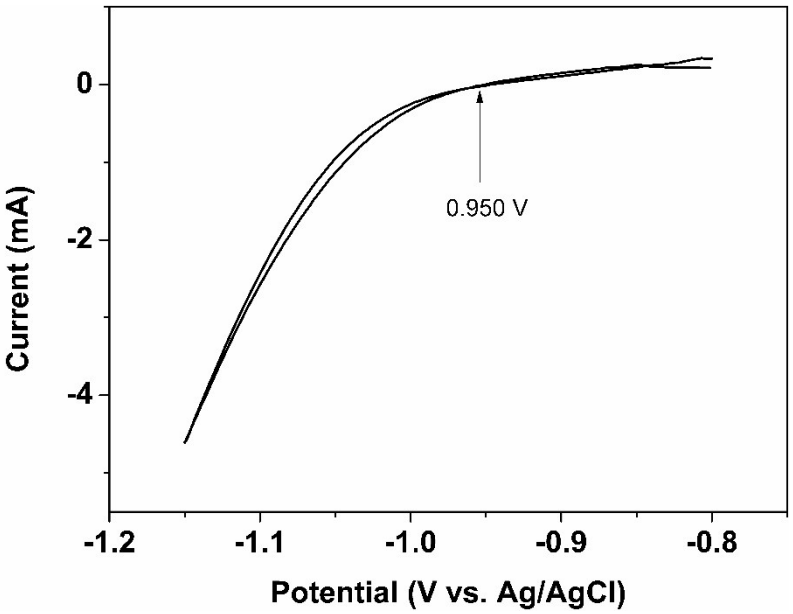

Figure S13. RHE calibration of the Ag/AgCl reference electrode in 0.1 M KOH.

Table S1. Specific surface areas (S) of the as-prepared SCFW perovskite oxide and commercial IrO_2 catalysts measured by nitrogen adsorption testing using the BET method.

Catalyst	S (m^2 g^{-1})
SCF	2.39
$SCFW_{0.05}$	1.43
$SCFW_{0.1}$	1.95
$SCFW_{0.2}$	2.07
$SCFW_{0.3}$	2.48
$SCFW_{0.4}$	2.92
$SCFW_{0.4}$-BM	7.60
IrO_2	139.80

Table S2. Comparison of the OER performance between our catalysts and the state-of-the-art catalysts.

Catalysts (electrolyte)	**Mass j ($mA\ mg^{-1}_{ox}$)**	**Specific j ($mA\ cm^{-2}_{ox}$)**	**$\eta_{@10\ mA\ cm^{-2}}$ (V)**	**Reference**
BSCF (0.1 M KOH)	10	1.3	0.510	S1
SNCF-BM (0.1 M KOH)	39	0.8	0.420	S2
NBSC-pPy (0.1 M KOH)	12	n.a.	0.420	S3
PBC (0.1 M KOH)	n.a.	n.a.	0.340	S4
$Ca_2Mn_2O_5$ (0.1 M KOH)	16	n.a.	>0.470	S5
SCP (0.1 M KOH)	5	0.1	0.480	S6
LCO-80 nm (0.1 M KOH)	8	0.2	0.490	S7
PBSCF-20 nm (0.1 M KOH)	200	1	0.358	S8

NF/oLCFO (0.1 M KOH)	n.a.	n.a.	0.350	S9
$L_{0.5}$BSCF/rGO (1.0 M KOH)	235	1.2	0.338	S10
$NdBaMn_2O_{5.5}$ (1.0 M KOH)	73	1.5	0.395	S11
G-FeCoW (1.0 M KOH)	n.a.	n.a.	0.223	S12
A-FeCoW (1.0 M KOH)	n.a.	n.a.	0.301	S12
SNCF-NR (1.0 M KOH)	182	0.4	0.370	S13
$SCFW_{0.4}$ (0.1 M KOH)	60	2.1	0.399	This work
$SCFW_{0.4}$-BM (0.1 M KOH)	143	1.9	0.357	This work
$SCFW_{0.4}$ (1.0 M KOH)	292	9.4	0.296	This work

References

[S1] G. Chen, W. Zhou, D. Guan, J. Sunarso, Y. Zhu, X. Hu, W. Zhang, Z. Shao, *Sci. Adv.* 2017, **3**, e1603206.

[S2] Y. Zhu, W. Zhou, Z.-G. Chen, Y. Chen, C. Su, M. O. Tadé, Z. Shao, *Angew. Chem. Int. Ed.* 2015, **54**, 3897.

[S3] D.-G. Lee, S. H. Kim, S. H. Joo, H-I. Ji, H. Tavassol, Y. Jeon, S. Choi, M.-H. Lee, C. Kim, S. K. Kwak, G. Kim, H.-K. Song, *Energy Environ. Sci.* 2017, **10**, 523.

[S4] A. Grimaud, K. J. May, C. E. Carlton, Y.-L. Lee, M. Risch, W. T. Hong, J. Zhou, Y. Shao-Horn, *Nat. Commun.* 2013, **4**, 2439.

[S5] J. Kim, X. Yin, K.-C. Tsao, S. Fang, H. Yang, *J. Am. Chem. Soc.* 2014, **136**, 14646.

[S6] Y. Zhu, W. Zhou, J. Sunarso, Y. Zhong, Z. Shao, *Adv. Funct. Mater.* 2016, **26**, 5862.

[S7] S. Zhou, X. Miao, X. Zhao, C. Ma, Y. Qiu, Z. Hu, J. Zhao, S. Lei, J. Zeng, *Nat. Commun.* 2016, **7**, 11510.

[S8] B. Zhao, L. Zhang, D. Zhen, S. Yoo, Y. Ding, D. Chen, Y. Chen, Q. Zhang, B. Doyle, X. Xiong, M. Liu, *Nat. Commun.* 2017, **8**, 14586.

[S9] B.-Q. Li, C. Tang, H.-F. Wang, X.-L. Zhu, Q. Zhang, *Sci. Adv.* 2016, **2**, e1600495.

[S10] B. Hua, M. Li, Y.-Q. Zhang, Y.-F. Sun, J.-L. Luo, *Adv. Energy Mater.* 2017, 1700666.

[S11] J. Wang, Y. Gao, D. Chen, J. Liu, Z. Zhang, Z. Shao, F. Ciucci, *ACS Catal.* 2018, **8**, 364.

[S12] B. Zhang, X. Zheng, O. Voznyy, R. Comin, M. Bajdich, M. García-Melchor, L. Han, J. Xu, M. Liu, L. Zheng, F.P. García de Arquer, C. T. Dinh, F. Fan, M. Yuan, E. Yassitepe, N. Chen, T. Regier, P. Liu, Y. Li, P. De Luna, A. Janmohamed, H.L. Xin, H. Yang, A. Vojvodic, E.H. Sargent, *Science* 2016, **352**, 333.

[S13] Y. Zhu, W. Zhou, Y. Zhong, Y. Bu, X. Chen, Q. Zhong, M. Liu, Z Shao, *Adv. Energy Mater.* 2017, 1602122.